JACS
JOURNAL OF THE AMERICAN CHEMICAL SOCIETY

Communication

pubs.acs.org/JACS

Artificial Solid Electrolyte Interphase-Protected Li_xSi Nanoparticles: An Efficient and Stable Prelithiation Reagent for Lithium-Ion Batteries

Jie Zhao,[†] Zhenda Lu,[†] Haotian Wang,[‡] Wei Liu,[†] Hyun-Wook Lee,[†] Kai Yan,[†] Denys Zhuo,[†] Dingchang Lin,[†] Nian Liu,[§] and Yi Cui*[,†,∥]

[†]Department of Materials Science and Engineering, Stanford University, Stanford, California 94305, United States

[‡]Department of Applied Physics, Stanford University, Stanford, California 94305, United States

[§]Department of Chemistry, Stanford University, Stanford, California 94305, United States

[∥]Stanford Institute for Materials and Energy Sciences, SLAC National Accelerator Laboratory, 2575 Sand Hill Road, Menlo Park, California 94025, United States

Supporting Information

ABSTRACT: Prelithiation is an important strategy to compensate for lithium loss in lithium-ion batteries, particularly during the formation of the solid electrolyte interphase (SEI) from reduced electrolytes in the first charging cycle. We recently demonstrated that Li_xSi nanoparticles (NPs) synthesized by thermal alloying can serve as a high-capacity prelithiation reagent, although their chemical stability in the battery processing environment remained to be improved. Here we successfully developed a surface modification method to enhance the stability of Li_xSi NPs by exploiting the reduction of 1-fluorodecane on the Li_xSi surface to form a continuous and dense coating through a reaction process similar to SEI formation. The coating, consisting of LiF and lithium alkyl carbonate with long hydrophobic carbon chains, serves as an effective passivation layer in the ambient environment. Remarkably, artificial-SEI-protected Li_xSi NPs show a high prelithiation capacity of 2100 mA h g^{-1} with negligible capacity decay in dry air after 5 days and maintain a high capacity of 1600 mA h g^{-1} in humid air (~10% relative humidity). Silicon, tin, and graphite were successfully prelithiated with these NPs to eliminate the irreversible first-cycle capacity loss. The use of prelithiation reagents offers a new approach to realize next-generation high-energy-density lithium-ion batteries.

Lithium-ion batteries have been widely used as the power supply in portable electronics over the last two decades.[1] Higher-energy-density Li-ion batteries are needed to expand their application toward electric vehicles.[2,3] High-capacity electrode materials as alternatives to Li intercalation compounds are therefore needed. Alloying anode materials such as silicon and tin are promising candidates because of their high theoretical specific capacities (4200 and 994 mA h g^{-1}, respectively).[4] However, the large volumetric change (>300%) during cycling usually results in rapid capacity decay as a result of high stress and mechanical damage. A common approach to address the issues associated with large volume changes is to use nanostructured materials such as porous materials,[5,6] nanowires and nanotubes,[7,8] and Si/C composites.[9] The drawback of these nanostructures is that their high surface area significantly increases solid electrolyte interphase (SEI) formation in the first and later cycles.[8,10] At the working potential of anodes, electrolytes are not stable and consequently are reduced on the anode surface to form the SEI, which consists of a complex composition of inorganic and organic lithium compounds.[11,12] SEI formation results in large irreversible capacity loss. The amorphous carbon used in the nanostructures further consumes Li.[9,13] Accordingly, the first-cycle Coulombic efficiency (1st cycle CE) of alloying anode materials is low, typically in the range of 50%−80%.[14,15] Although the 1st cycle CE of commercial graphite is consistently >90%, the capacity of the anode is usually 10% greater than that of the cathode to reduce the probability of Li deposition, which further exacerbates the irreversible capacity loss of the full cell.[16,17] As common Li metal oxide cathodes have relatively low specific capacities (<200 mA h g^{-1}),[18] the overall energy density of the battery cell is largely reduced if the ratio of the cathode is increased to compensate for the irreversible capacity in the anode. In addition, it may increase the probability of Li deposition, presenting a safety concern for the battery.[19] A prelithiation reagent as a secondary source of Li is therefore attractive for batteries.

Currently, the only commercial prelithiation reagent in powder form is microscale stabilized lithium metal powder (SLMP) (FMC Lithium Corp.), which effectively compensates for the first-cycle irreversible capacity loss of different anode materials, such as SiO and Si−CNT composites.[20,21] However, it is difficult to synthesize SLMP in research laboratories, and other practical challenges still remain to be addressed.[17] To minimize the disturbance of the whole structure of the electrodes by prelithiation reagents, we recently explored Li_xSi nanoparticles (NPs).[22] Because of the chemical reactivity of Li_xSi, an appreciable amount of capacity is sacrificed to form a Li_2O passivation layer to stabilize Li_xSi as Li_xSi−Li_2O core−shell NPs. However, Li_xSi−Li_2O NPs maintain their capacity in air with low

Received: April 30, 2015

DOI: 10.1021/jacs.5b04526
J. Am. Chem. Soc. XXXX, XXX, XXX−XXX

relative humidity (RH) for only relatively short durations, which limits their potential use in large-scale applications. Therefore, nanoscale prelithiation reagents with higher capacity and improved stability should be explored. Here we report a facile reaction process utilizing the highly reactive nature of Li_xSi NPs to reduce 1-fluorodecane, thereby producing a continuous and dense coating over the NPs (Figure 1a). The synthesis is inspired

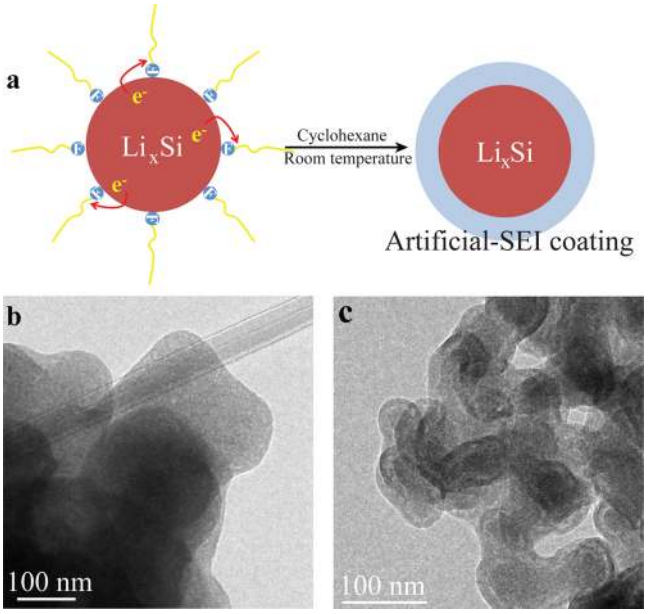

Figure 1. (a) Schematic diagram of the artificial SEI coating formed by reduction of 1-fluorodecane on the surface of Li_xSi NPs in cyclohexane. (b, c) TEM images of Li_xSi NPs (b) before and (c) after coating.

by the process of SEI formation in battery anodes. The conformal coating, consisting of LiF and lithium alkyl carbonate with long hydrophobic carbon chains, effectively suppresses the reactivity of Li_xSi NPs under ambient conditions, allowing safe storage and handling. The passivated NPs can be reactivated by contact with the electrolyte during battery fabrication. These artificial-SEI-protected Li_xSi NPs exhibit a high capacity of ~2100 mA h g^{-1} and can be mixed with various anode materials during slurry processing to eliminate first-cycle irreversible capacity loss. These particles show negligible capacity decay in dry air after 5 days and still exhibit a capacity of 1600 mA h g^{-1} in humid air (~10% RH) after 6 h.

Artificial-SEI-protected Li_xSi NPs were prepared via two synthetic steps. First, crystalline Li_xSi NPs were synthesized as our previous study[22] by heating a stoichiometric mixture (1:4.4) of Si NPs and Li metal foil at 200 °C under mechanical stirring inside a tantalum crucible at 200 rpm for 3 days in a glovebox (Ar atmosphere, <1.2 ppm O_2 and <0.1 ppm H_2O). Figure S1 in the Supporting Information shows a digital photograph of 1 g of Li_xSi NPs synthesized through this process, indicating the potential for mass production in industry. As-synthesized NPs were characterized by transmission electron microscopy (TEM) and scanning electron microscopy (SEM). Care had been taken to limit the electron beam exposure time during image acquisition in order to minimize beam damage to the sample. The TEM and SEM images (Figures 1b and S2c) show that the surface of the synthesized Li_xSi NPs is clean and smooth. To prepare an inert passivation layer, we explored fluorinated compounds as the precursor. The surfactant-like molecule 1-fluorodecane was selected because of its excellent processability in nonpolar solvents such as cyclohexane, which allowed us to prepare the artificial SEI layer in a nonpolar solvent, eliminating the possible capacity loss of Li_xSi in polar solvents.[22] In the second step, Li_xSi NPs were added to 1-fluorodecane dissolved in anhydrous cyclohexane and reacted for 2 h at room temperature. Dissolved 1-fluorodecane was directly reduced on the surface of these NPs to form a conformal coating (Figures 1c and S2f). The selective and self-limiting reaction ensures a uniform and continuous coating on the surface. The TEM image indicated that each individual particle was wrapped in a uniform ~13 nm thick coating. The dispersion of NPs was also improved after coating. Doubling the concentration of 1-fluorodecane in cyclohexane increased the thickness to ~30 nm (Figure S3b), indicating the tunability of the coating layer thickness.

Compositional analysis of the core−shell NPs was acquired by X-ray diffraction (XRD), energy-dispersive spectroscopy (EDS), X-ray photoelectron spectroscopy (XPS), electron energy loss spectroscopy (EELS), and Raman spectroscopy. All of the peaks in the XRD pattern (Figure 2a) could be indexed as $Li_{21}Si_5$ (PDF

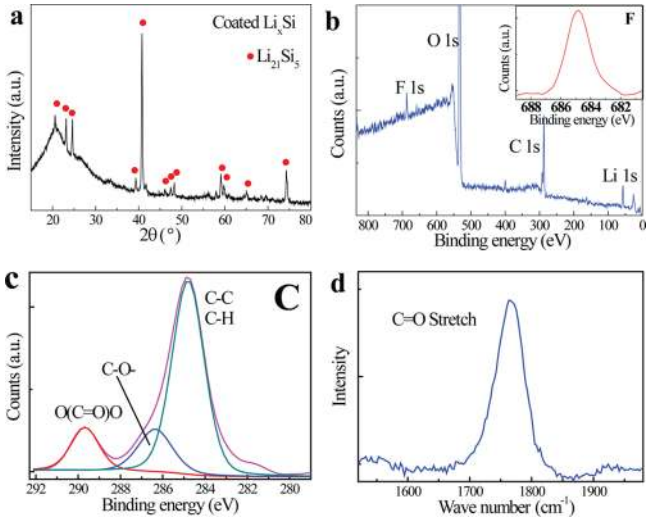

Figure 2. (a) XRD pattern of artificial-SEI-coated Li_xSi NPs sealed in Kapton tape. (b) XPS of artificial-SEI-coated Li_xSi NPs. Corresponding high-resolution XPS spectrum around F 1s peak region is shown in the inset. (c) High-resolution XPS spectra of C 1s. (d) Raman spectrum reveals the peak near 1762 cm^{-1} as the stretching vibration mode of C═O.

no. 00-018-747),[23] indicating a crystalline Li_xSi core and an amorphous coating layer. TEM-EDS performed on a cluster of coated Li_xSi NPs confirmed the presence of C, O, F, and Si (Figure S4). Consistently, XPS (Figure 2b) confirmed the chemical composition of the coating layer with the presence of F, O, C, and Li. The binding energies were calibrated with respect to the C 1s peak at 284.8 eV. The Si 2p peak typically observed at around 100 eV, however, is absent in the spectrum, suggesting excellent encapsulation of the coating, which masks the NPs from surface-sensitive compositional characterization. The F 1s spectrum (Figure 2b inset) contains a single peak at 684.9 eV, supporting the presence of LiF.[24] The shape of the Li K-edge EELS spectrum (Figure S5) also confirmed the formation of LiF.[25] Besides the strong hydrocarbon peak, XPS showed two main C peaks at 289.8 and 286.4 eV, corresponding to −O(C═O)O− and −C−O−, respectively (Figure 2c).[12,26] The XPS spectra also revealed a Li 1s peak at 55.2 eV and an O 1s peak at 531.4 eV, matching the peak positions for lithium alkyl carbonate

DOI: 10.1021/jacs.5b04526
J. Am. Chem. Soc. XXXX, XXX, XXX−XXX

(Figure S7).[26] The peak assignments were further supported by Raman spectroscopy (Figure 2d). The Raman spectrum reveals a strong peak at 1762 cm^{-1} that corresponds to the C═O stretching vibration mode, with a peak position similar to that of Li_2CO_3.[27,28]

We propose a reaction pathway for the generation of LiF and lithium alkyl carbonate on the surface of Li_xSi NPs. Similar to the mechanism for the preparation of butyllithium,[29] single electron transfer from Li_xSi to C−F in 1-fluorodecane forms a C radical and F^-, and a second electron transfer converts the C radical into a carbanion (reaction 1). Alkyllithium is highly volatile and spontaneously reacts with trace amounts of O_2 and CO_2 in the glovebox to form lithium decyl carbonate (reaction 2). The detailed reaction mechanism is shown in Figure S6.

$$F{-}(CH_2)_9CH_3 \xrightarrow{Li_xSi} LiF + Li{-}(CH_2)_9CH_3 \quad (1)$$

$$Li{-}(CH_2)_9CH_3 \xrightarrow{O_2/CO_2} Li{-}OC(=O)O{-}(CH_2)_9CH_3 \quad (2)$$

To evaluate the electrochemical performance, half-cells were fabricated with Li metal as the counter electrode. Active materials were mixed with carbon black and polyvinyldifluoride (PVDF) in tetrahydrofuran to form a slurry, which was then drop-cast on copper foil and dried under vacuum. Because of the high chemical reactivity of Li_xSi, solvents with higher polarity should be avoided for slurry preparation. As shown in Figure S8a, the extraction capacity of Li_xSi is 2235 mA h g^{-1}, whereas that of the coated Li_xSi is 2078 mA h g^{-1}, indicating that about 10% of the active Li is consumed to form the coating layer (the specific capacity is estimated on the basis of the mass of Si in the electrode: 1 C = 4.2 A/g of Si). Aside from a tiny loss of capacity, this coating has beneficial effects on the electrochemical performance, as its chemical composition resembles the typical SEI formed in the battery.[11] Coated Li_xSi NPs were first lithiated to 0.01 V and then delithiated to 1 V at a rate of C/50 (Figure 3a). The open-circuit voltage (OCV) of 0.27 V is significantly lower than that of crystalline Si. The large plateau at 0.4 V confirmed the crystalline nature of Li_xSi. Figure 3b demonstrates the use of coated Li_xSi NPs as a prelithiation reagent to compensate for the irreversible capacity loss of Si NPs. Coated Li_xSi NPs were mixed with Si NPs, super P, and PVDF in a weight ratio of 10:55:20:15 in a slurry to form the working electrodes. Coated Li_xSi NPs were activated by contact with the carbonate electrolyte, supplying additional Li ions to the anode for the formation of the SEI layer and partial lithiation of the Si NPs. After a cell was assembled, it took about 6 h for the electrode to reach equilibrium as determined by the stabilized potential of the anode. As shown in Figure 3b, the OCV of 0.34 V is significantly lower than that of crystalline Si, indicating partial prelithiation of the Si NPs. The 1st cycle CE increased from 76.1% to 96.8%, confirming effective compensation for the large irreversible capacity loss in conventional Si NP anodes with the extra capacity from the coated Li_xSi NPs. Similarly, tin NPs were successfully prelithiated with coated Li_xSi, achieving a high 1st cycle CE up to 98.7% (tin:coated Li_xSi = 60:5 w/w; Figure S9); without prelithiation, tin NPs have a 1st cycle CE of only 77.7%. The theoretical capacity of Si is about 10 times that of graphite.[9] Hence, it would be highly effective to prelithiate graphite with a small amount of coated Li_xSi. The graphite control cell was measured in the voltage window of 0.005−1.5 V. The blue voltage profile in Figure 3c reveals an obvious plateau at around 0.7 V, corresponding to formation of the SEI on the first cycle. The

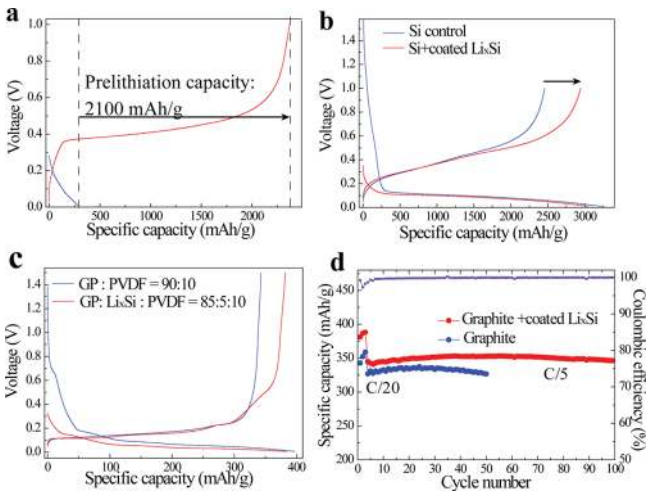

Figure 3. (a) First-cycle galvanostatic discharge/charge profiles of artificial-SEI-coated Li_xSi NPs. (b) First-cycle voltage profiles of Si NPs/coated Li_xSi composite (55:10 w/w) and Si NPs control cells. The capacity is based on the total mass of Si in the electrodes. (c) First-cycle voltage profiles of graphite/coated Li_xSi composite (85:5 w/w) and graphite control cells. (d) Cycling performance of graphite/coated Li_xSi composite and graphite control cells at C/20 for the first three cycles and C/5 for the following cycles (1 C = 0.372 A/g; the capacity is based on the mass of graphite and Si in coated Li_xSi NPs). The purple line is the Coulombic efficiency of the graphite/coated Li_xSi composite.

incorporation of a small amount of coated Li_xSi (graphite:coated Li_xSi = 85:5 w/w) improved the 1st cycle CE from 87.4% to 99.2%. Because of their small size, the added Li_xSi NPs are expected to be embedded in the interstices of graphite microparticles. Since Li_xSi is already in its expanded state, sufficient space has been created during electrode fabrication. The Li_xSi NPs will not squeeze each other during cycling. Therefore, coated Li_xSi NPs exhibit improved cyclability compared with Si NPs (Figure S10). Accordingly, with the introduction of coated Li_xSi (Figure 3d), graphite anodes exhibit consistent higher capacity and good cycling at C/20 for the first three cycles and C/5 for the following cycles (1 C = 372 mA/g; the capacity is based on both graphite and Si in Li_xSi). This suggests that the Li_xSi NPs are unlikely to affect the stability of the anode materials during cycling. Aside from the improved 1st cycle CE, the CEs of the subsequent cycles are comparable to those of cells without Li_xSi (Figure S11).

To evaluate the dry-air stability, coated Li_xSi NPs were stored in a dry room (dew point = −50 °C) for different numbers of days. After 5 days in dry air, the coated Li_xSi NPs still exhibited a high capacity of 1921 mA h g^{-1}, which is only an 8% decay from the initial capacity (Figure 4a). In addition, the capacity decay in dry air was much slower for coated NPs than pristine NPs (Figure 4a inset), confirming that the artificial SEI coating slowed the NPs' side reaction in dry air. To further explore the stability in humid air, coated Li_xSi NPs were stored in air with different humidity levels for 6 h. The remaining capacity was tested by delithiating the cells to 1 V (Figure 4b). After exposure to humid air with 10% RH, the coated Li_xSi NPs still exhibited a high extraction capacity of 1604 mA h g^{-1}. The first-cycle voltage profile of the composite anode (graphite/coated Li_xSi = 85:5 w/w; Figure S12) indicated that these Li_xSi NPs were still active enough to prelithiate graphite, yielding a high 1st cycle CE of 96.7%. For humidity levels higher than 20% RH, the Li extraction capacity showed a large drop after the 6 h storage period.

DOI: 10.1021/jacs.5b04526
J. Am. Chem. Soc. XXXX, XXX, XXX−XXX

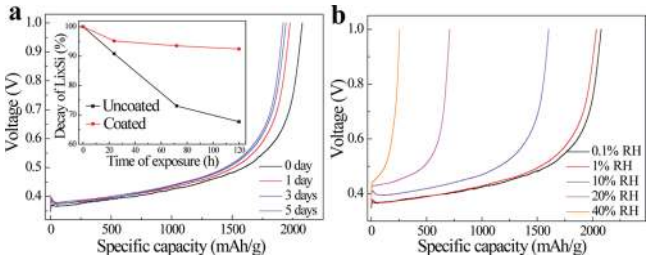

Figure 4. (a) Extraction capacities of artificial-SEI-coated NPs exposed to dry air for varying periods of time. The inset shows the change in capacity as a function of exposure time. (b) Extraction capacities of artificial-SEI-coated NPs exposed to air for 6 h at different humidity levels.

However, this humidity level is higher than battery electrode fabrication conditions in industry. XRD (Figure S13) demonstrated the different reactivities of coated and uncoated Li_xSi in moisture. Peaks corresponding to LiOH and Li_2O appear in the XRD pattern of uncoated Li_xSi stored in air with 10% RH for only 2 h. There is no obvious change in the XRD pattern for coated Li_xSi NPs. LiF provides an excellent passivation effect compared with other lithium salts due to the limited solubility of LiF in water (0.134 g/100 mL at 25 °C).[30] The solubility is about 1 order of magnitude lower than that of Li_2CO_3 (1.29 g/100 mL), the coating layer used in SLMP. In contrast, some lithium salts (e.g., Li_2O) react violently with water. LiF, along with lithium alkyl carbonate with long hydrophobic carbon chains, slows the reaction with O_2 and water vapor in the ambient environment.

In conclusion, we have developed a two-step process for preparing artificial-SEI-protected Li_xSi NPs. The uniform and continuous coating, consisting of LiF and lithium decyl carbonate, slows side reactions under ambient conditions. Therefore, the coated Li_xSi NPs show negligible capacity decay in dry air after 5 days and exhibit a high capacity of ~1600 mA h g^{-1} at 10% RH, indicating that they are potentially compatible with the industrial battery fabrication environment. It has been shown that both alloying and intercalation anode materials can be effectively prelithiated with coated Li_xSi to counteract first-cycle capacity loss, and this approach is applicable to other advanced electrode systems involving components of nanomaterials. Thus, incorporation of coated Li_xSi NPs is a promising approach that may enable the commercial implementation of high-capacity nanostructured materials with large first-cycle irreversible capacity loss, which is a significant step toward high-energy-density Li-ion batteries.

■ ASSOCIATED CONTENT

Supporting Information

Complete experimental details and additional characterizations. The Supporting Information is available free of charge on the ACS Publications website at DOI: 10.1021/jacs.5b04526.

■ AUTHOR INFORMATION

Corresponding Author

*yicui@stanford.edu

Notes

The authors declare no competing financial interest.

■ ACKNOWLEDGMENTS

We acknowledge the support from the Assistant Secretary for Energy Efficiency and Renewable Energy, Office of Vehicle Technologies, Battery Materials Research Program, U.S. Department of Energy. D.Z. acknowledges the support through a National Science Foundation Graduate Fellowship.

■ REFERENCES

(1) Whittingham, M. S. *MRS Bull.* **2008**, *33*, 411−419.
(2) Palacin, M. R. *Chem. Soc. Rev.* **2009**, *38*, 2565−2575.
(3) Bruce, P. G.; Freunberger, S. A.; Hardwick, L. J.; Tarascon, J. M. *Nat. Mater.* **2012**, *11*, 19−29.
(4) McDowell, M. T.; Lee, S. W.; Nix, W. D.; Cui, Y. *Adv. Mater.* **2013**, *25*, 4966−4984.
(5) Liu, N.; Huo, K. F.; McDowell, M. T.; Zhao, J.; Cui, Y. *Sci. Rep.* **2013**, *3*, No. 1919.
(6) Li, X. L.; Gu, M.; Hu, S. Y.; Kennard, R.; Yan, P. F.; Chen, X. L.; Wang, C. M.; Sailor, M. J.; Zhang, J.-G.; Liu, J. *Nat. Commun.* **2014**, *5*, No. 4105.
(7) Chan, C. K.; Peng, H. L.; Liu, G.; McIlwrath, K.; Zhang, X. F.; Huggins, R. A.; Cui, Y. *Nat. Nanotechnol.* **2008**, *3*, 31−35.
(8) Wu, H.; Chan, G.; Choi, J. W.; Ryu, I.; Yao, Y.; McDowell, M. T.; Lee, S. W.; Jackson, A.; Yang, Y.; Hu, L. B.; Cui, Y. *Nat. Nanotechnol.* **2012**, *7*, 309−314.
(9) Liu, N.; Lu, Z. D.; Zhao, J.; McDowell, M. T.; Lee, H. W.; Zhao, W. T.; Cui, Y. *Nat. Nanotechnol.* **2014**, *9*, 187−192.
(10) Szczech, J. R.; Jin, S. *Energy Environ. Sci.* **2011**, *4*, 56−72.
(11) Xu, K. *Chem. Rev.* **2004**, *104*, 4303−4417.
(12) Schroder, K. W.; Celio, H.; Webb, L. J.; Stevenson, K. J. *J. Phys. Chem. C* **2012**, *116*, 19737−19747.
(13) Ko, M.; Chae, S.; Jeong, S.; Oh, P.; Cho, J. *ACS Nano* **2014**, *8*, 8591−8599.
(14) Lee, W. J.; Hwang, T. H.; Hwang, J. O.; Kim, H. W.; Lim, J.; Jeong, H. Y.; Shim, J.; Han, T. H.; Kim, J. Y.; Choi, J. W.; Kim, S. O. *Energy Environ. Sci.* **2014**, *7*, 621−626.
(15) Jung, D. S.; Hwang, T. H.; Park, S. B.; Choi, J. W. *Nano Lett.* **2013**, *13*, 2092−2097.
(16) Yoshio, M.; Wang, H. Y.; Fukuda, K. *Angew. Chem., Int. Ed.* **2003**, *42*, 4203−4206.
(17) Wang, L.; Fu, Y. B.; Battaglia, V. S.; Liu, G. *RSC Adv.* **2013**, *3*, 15022−15027.
(18) Li, Y. Y.; El Gabaly, F.; Ferguson, T. R.; Smith, R. B.; Bartelt, N. C.; Sugar, J. D.; Fenton, K. R.; Cogswell, D. A.; Kilcoyne, A. L. D.; Tyliszczak, T.; Bazant, M. Z.; Chueh, W. C. *Nat. Mater.* **2014**, *13*, 1149−1156.
(19) Zheng, G. Y.; Lee, S. W.; Liang, Z.; Lee, H. W.; Yan, K.; Yao, H. B.; Wang, H. T.; Li, W. Y.; Chu, S.; Cui, Y. *Nat. Nanotechnol.* **2014**, *9*, 618−623.
(20) Zhao, H.; Wang, Z.; Lu, P.; Jiang, M.; Shi, F.; Song, X.; Zheng, Z.; Zhou, X.; Fu, Y.; Abdelbast, G.; Xiao, X.; Liu, Z.; Battaglia, V. S.; Zaghib, K.; Liu, G. *Nano Lett.* **2014**, *14*, 6704−6710.
(21) Forney, M. W.; Ganter, M. J.; Staub, J. W.; Ridgley, R. D.; Landi, B. J. *Nano Lett.* **2013**, *13*, 4158−4163.
(22) Zhao, J.; Lu, Z. D.; Liu, N. A.; Lee, H.-W.; McDowell, M. T.; Cui, Y. *Nat. Commun.* **2014**, *5*, No. 5088.
(23) Nesper, R.; von Schnering, H. G. *J. Solid State Chem.* **1987**, *70*, 48−57.
(24) Shao, M. W.; Cheng, L.; Zhang, X. H.; Ma, D. D. D.; Lee, S. T. *J. Am. Chem. Soc.* **2009**, *131*, 17738−17739.
(25) Wang, F.; Graetz, J.; Moreno, M. S.; Ma, C.; Wu, L. J.; Volkov, V.; Zhu, Y. M. *ACS Nano* **2011**, *5*, 1190−1197.
(26) Dedryvere, R.; Gireaud, L.; Grugeon, S.; Laruelle, S.; Tarascon, J. M.; Gonbeau, D. *J. Phys. Chem. B* **2005**, *109*, 15868−15875.
(27) Visser, T.; Vandermaas, J. H. *J. Raman Spectrosc.* **1978**, *7*, 125−129.
(28) Brooker, M. H.; Wang, J. F. *Spectrochim. Acta, Part A* **1992**, *48*, 999−1008.
(29) Wilke, G. *Angew. Chem., Int. Ed.* **2003**, *42*, 5000−5008.
(30) Stubblefield, C. B.; Bach, R. O. *J. Chem. Eng. Data* **1972**, *17*, 491−492.

DOI: 10.1021/jacs.5b04526
J. Am. Chem. Soc. XXXX, XXX, XXX−XXX